NANO LETTERS

pubs.acs.org/NanoLett

Letter

Nonlinear Stiffness and Nonlinear Damping in Atomically Thin MoS_2 Nanomechanical Resonators

Tahmid Kaisar,[†] Jaesung Lee,[†] Donghao Li, Steven W. Shaw, and Philip X.-L. Feng*

Cite This: https://doi.org/10.1021/acs.nanolett.2c02629

Read Online

ACCESS | Metrics & More | Article Recommendations | Supporting Information

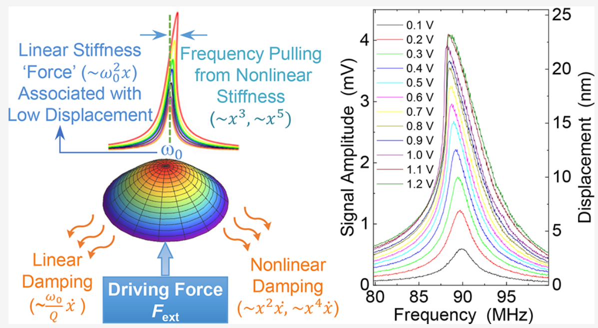

ABSTRACT: We report on experimental measurements and quantitative analyses of nonlinear dynamic characteristics in ultimately thin nanomechanical resonators built upon single-layer, bilayer, and trilayer (1L, 2L, and 3L) molybdenum disulfide (MoS_2) vibrating drumhead membranes. This synergistic study with calibrated measurements and analytical modeling on observed nonlinear responses has led to the determination of nonlinear damping and stiffness coefficients at *cubic* and *quintic* orders for these two-dimensional (2D) resonators operating in the very high frequency (VHF) band (up to ~90 MHz). We find that the *quintic* force can be ~20% of the Duffing force at larger amplitudes, and thus, it generally cannot be ignored in a nonlinear dynamics analysis. This study provides the first quantification of nonlinear damping and frequency detuning characteristics in 2D semiconductor nanomechanical resonators and elucidates their origins and dependency on engineerable parameters, setting a foundation for future exploration and utilization of the rich nonlinear dynamics in 2D nanomechanical systems.

KEYWORDS: *Resonator, Nonlinearity, Duffing, Quintic, Nonlinear Damping, 2D Materials*

Miniaturized nonlinear resonators, particularly those made in micro/nanoelectromechanical systems (M/NEMS), have received growing interest in recent years because of their small sizes and related advantages, including their nimble tunability, which opens the door to novel applications.[1,2] Nonlinearity plays an increasingly important role in describing the dynamic behavior of these devices,[3−8] due to their relatively small sizes and high vibration amplitudes. This has an impact on the performance of such resonators, for example, in engineering the quantum behavior of M/NEMS,[9] force and mass sensing,[10] and radio frequency (RF) signal processing applications.[11−13] These applications require very high precision, which necessitates performance improvements associated with high quality (Q) factors, large signal-to-noise ratio,[14] very low phase noise,[15] etc. To meet these demands, M/NEMS resonators are frequently operated at relatively large vibration amplitudes that can induce the onset of nonlinearity. To analyze and predict the nonlinear dynamic behavior of these systems, it is often necessary to use a model expressed in terms of coefficients that account for both nonlinear damping[16−18] and nonlinear stiffness.[19] Insights gained from single-mode models with such terms will be essential for describing dynamics involving more degrees of freedom (DoFs), such as arrays of devices with coupling or interconnections which can be used, for example, for noise reduction and demonstrating intrinsic localized modes.[20,21]

To fully realize the benefits of the emerging two-dimensional (2D) NEMS resonant devices enabled by atomically thin crystals, it is important to thoroughly investigate their nonlinear behavior. During recent years, 2D NEMS have exhibited many intriguing features,[1,22−24] e.g., they show strong nonlinear mode coupling[25] between vibrational modes, which can result in internal resonances with unique and potentially useful properties.[26] Nonlinear damping in one-dimensional (1D) carbon nanotube and 2D graphene resonators has been studied,[16] and $Q \sim 100{,}000$ (at $T = 90$ mK) has been achieved for graphene resonators by manipulating this nonlinear nature of damping.[16] Though nonlinear stiffness of 2D NEMS has been studied in literature,[16,27,28] to date, however, there has been no experimental demonstration and investigation of nonlinear damping in 2D semiconductor NEMS resonators.

In this paper, we present nonlinearity measurements and analyses of atomically thin MoS_2 2D nanomechanical resonators. In comparison to their 1D NEMS predecessors, these 2D atomic layer devices exhibit wide dynamic ranges[29]

Received: July 5, 2022
Revised: October 26, 2022
Published: December 8, 2022

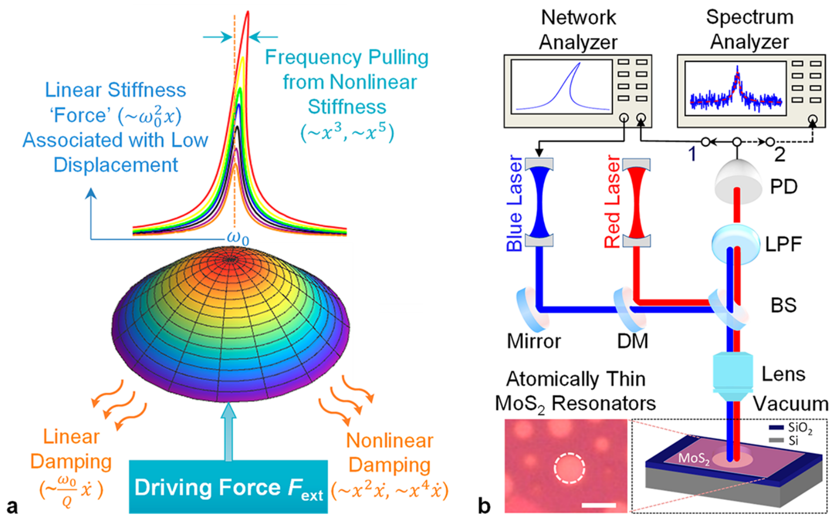

Figure 1. Conceptual illustration of nonlinear effects and optical interferometry measurement system. (a) Illustration showing nonlinear damping and stiffness associated with mode shape due to increasing displacement of the device. (b) Laser optical interferometry measurement scheme, including photodetector (PD), long pass filter (LPF), beam splitter (BS), dichroic mirror (DM), and device image identified by optical microscopy (inset, scale bar: 2 μm). The output of the photodetector is connected to position 1 while measuring driven resonance and connected to position 2 during undriven thermomechanical noise measurement.

(often ~70−110 dB), making them promising candidates for ultrasensitive resonant transduction and ultralow-power information processing applications. We have found that the observed behavior of the present devices requires the inclusion of *nonlinear damping effects* and *higher-order nonlinear stiffness coefficients* in analysis and modeling. Because of the various length scales and device sizes, estimating these nonlinear coefficients in vibrating systems is often difficult, and it necessitates understanding the dynamics of the system using standard models. This work aims to extract the values of linear and nonlinear damping coefficients, along with linear, Duffing, and quintic stiffness terms, for single-layer and few-layer MoS_2 2D nanomechanical resonators.

The conceptual illustration and the optical interferometry measurement system (Supporting Information S2) are shown in Figure 1. As depicted in Figure 1a, the input energy to the device is dissipated through linear and nonlinear damping forces. Increased input driving force induces large displacement in the MoS_2 device, resulting in observed effects from Duffing and quintic nonlinearities, which in turn cause detuning in the resonant frequency.

Considering the fundamental flexural mode of the 2D vibrating drumheads, we assume a single DoF system of a driven, damped harmonic resonator with eigenfrequency ω_0 and with nonlinear characteristics (Figure 1a). Beyond the regular treatment of nonlinear resonators, where the equation of motion includes a Q factor associated with linear damping ($\sim(\omega_0\dot{x}/Q)$), a linear restoring force ($k_{eff}x = m_{eff}\omega_0{}^2x$), and a Duffing nonlinearity (k_3x^3), here we also consider higher-order nonlinearities, specifically, a quintic stiffness nonlinearity (k_5x^5), and higher-order, nonlinear damping effects ($\sim x^2\dot{x}$ and $\sim x^4\dot{x}$ terms), as illustrated in Figure 1a. We focus on the use of this model to quantitively examine the nonlinear dynamics of atomically thin circular membrane NEMS resonators made of one to three molecular layers (1L to 3L) of MoS_2 crystals. The governing equation of motion that includes these higher-order nonlinearities is

$$\ddot{x} + 2(\zeta_1 + \zeta_3x^2 + \zeta_5x^4)\omega_0\dot{x} + \omega_0{}^2x + \frac{k_3}{m_{eff}}x^3 + \frac{k_5}{m_{eff}}x^5 = \frac{F_{ext}}{m_{eff}} \quad (1)$$

Here, $\omega_0 = 2\pi f_0$ is the angular eigenfrequency of the mode of interest, m_{eff} is the effective modal mass, $F_{ext}(t) = F\cos(\omega t)$ is the external driving force, k_3 [unit: N m^{-3}] and k_5 [unit: N m^{-5}] are the coefficients of the conservative Duffing and quintic nonlinearities, respectively, ζ_1 is the linear damping coefficient, and ζ_3 [unit: m^{-2}] and ζ_5 [unit: m^{-4}] are the third and fifth order nonlinear damping coefficients, respectively. The linear damping coefficient ζ_1 describes the resonator decay at small vibration amplitudes and is inversely proportional to the Q of the resonator, $\zeta_1 = 1/(2Q)$. The nonlinear stiffness terms associated with k_3 and k_5 create an amplitude-dependent frequency shift and attendant bending of the frequency response curve near resonance. The nonlinear damping terms associated with ζ_3 and ζ_5 result in an amplitude-dependent decay rate and an attendant nonexponential decay. The overall decay of the oscillation amplitude can be determined by the terms proportional to ζ_1, ζ_3, and ζ_5.

The method of averaging is used to obtain equations that approximate the slow variation of the amplitude and phase of $x(t)$ under the assumptions of small, near-resonant drive, small damping, and weak nonlinear effects.[30] The van der Pol transformation is first applied to move to a rotating frame of reference in which the equations for the amplitude and phase are suitable equations for averaging (Supporting Information S5). Specifically, we define

$$x(t) = r(t)\cos[\omega t + \varphi(t)],\ \dot{x}(t) = -\omega r(t)\sin[\omega t + \varphi(t)] \quad (2)$$

and the associated constraint equation to satisfy the above transformation is $\dot{r}(t)\cos[\omega t + \varphi(t)] - r(t)\dot{\varphi}(t)\sin[\omega t + \varphi(t)] = 0$. In the above equations, $r(t)$ and $\varphi(t)$ are the time-varying amplitude and phase of $x(t)$. We define frequency

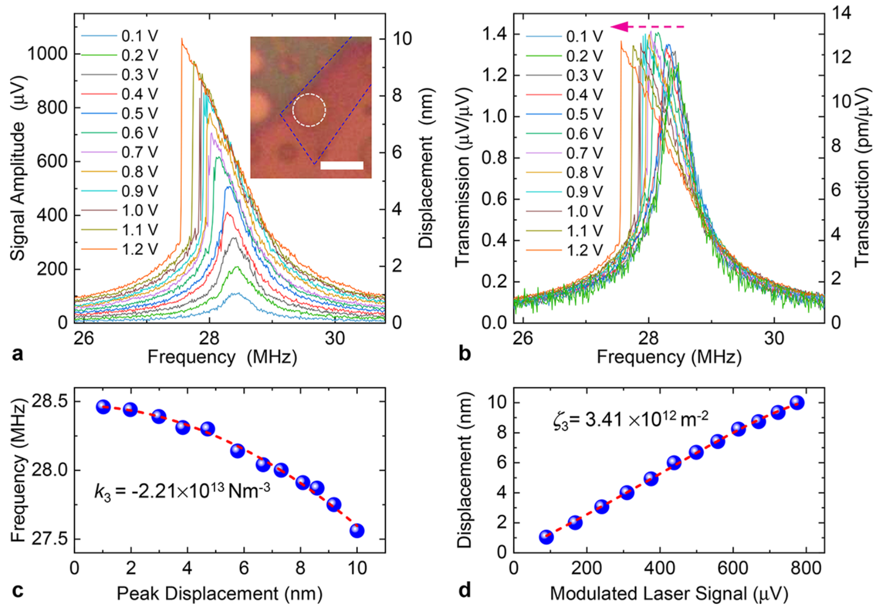

Figure 2. Determining nonlinear damping and stiffness coefficients of a 1L MoS_2 resonator. (a) Signal amplitude and peak displacement versus frequency, including device image identified by optical microscopy (inset, scale bar: 2 μm). (b) Transmission and transduction responsivity (gain) versus frequency. The dashed arrow indicates frequency pulling of the peak amplitude arising from nonlinear stiffness and damping. The peak transmission does not vary appreciably, indicating essentially linear damping. (c) Frequency versus peak displacement (backbone curve). The red dashed line is a fit to eq 6. (d) Peak displacement versus modulated laser signal. The red dashed line is a fit to eq 7.

detuning as $\Delta\omega = \omega - \omega_0$ and assume $\frac{\Delta\omega}{\omega} \ll 1$, so that $\frac{\omega^2 - \omega_0^2}{\omega} \approx 2\Delta\omega$. Then, we average time over one period, $2\pi/\omega$, assuming that $r(t)$ and $\varphi(t)$ do not vary appreciably over one period. After implementing the detuning definition and substituting eq 2 and its derivatives to eq 1, imposing the constraint equation, and averaging, eq 1 is converted to the following equations

$$\dot{r} = -r\zeta_1\omega_0 - \frac{1}{4}r^3\zeta_3\omega_0 - \frac{1}{8}r^5\zeta_5\omega_0 - \frac{F\sin\varphi}{2\omega_0} \quad (3)$$

$$\dot{\varphi} = \frac{3k_3r^2}{8\omega_0} + \frac{5k_5r^4}{16\omega_0} - \Delta\omega - \frac{F\cos\varphi}{2r\omega_0} \quad (4)$$

The free vibration dynamics are determined by setting $F = 0$, and $\Delta\omega = 0$, for which the amplitude-dependent decay rate and frequency pulling are evident in eqs 3 and 4, respectively. For the driven steady-state conditions, let $\dot{r} = 0$ and $\dot{\varphi} = 0$, and from this, one can apply a trigonometric identity on $F\sin\varphi$ and $F\cos\varphi$ to eliminate φ, yielding an implicit condition for the steady-state amplitude as

$$\Delta\omega = \frac{3k_3r^2}{8\omega_0} + \frac{5k_5r^4}{16\omega_0} \pm \frac{1}{\omega_0 r}\sqrt{\frac{F^2}{4\omega_0^2} - \left(r\zeta_1\omega_0 + \frac{1}{4}r^3\zeta_3\omega_0 + \frac{1}{8}r^5\zeta_5\omega_0\right)^2} \quad (5)$$

The terms before the $\pm$ sign determine the backbone curve (the undriven amplitude dependent instantaneous frequency Ω during ringdown), while the terms inside the square root determine the peak amplitude, r_p, specifically,

$$\Omega = \omega_0 + \dot{\varphi} = \omega_0 + \frac{3k_3r^2}{8\omega_0 m_{eff}} + \frac{5k_5r^4}{16\omega_0 m_{eff}} \quad (6)$$

$$\frac{F}{m_{eff}} = 2\zeta_1\omega_0^2 r_p + \frac{1}{2}\zeta_3\omega_0^2 r_p^3 + \frac{1}{4}\zeta_5\omega_0^2 r_p^5 \quad (7)$$

where eq 6 corresponds to the *backbone curve* that can be used to determine stiffness parameters by measuring the instantaneous frequency as r decays. The peak of the frequency response occurs for $\varphi = \pi/2$ in the driven system and the frequency at the peak tracks along the backbone curve as the drive level is varied. Eq 7 expresses how the peak amplitude r_p depends on the nonlinear damping parameters and can be used to estimate them from forced response data.[17] These results provide an alternative method to the ringdown approach for measuring nonlinear stiffness and damping.[7]

RESULTS AND DISCUSSIONS

Figure 2 shows signal amplitude (in both transduced voltage signal and device displacement), transmission and transduction responsivity, backbone curve, and curve fitting analysis of a 1L MoS_2 resonator (device 1). The device has diameter $d = 1.5$ μm, thickness $h = 0.7$ nm, stiffness $k_{eff} = 0.0539$ N/m, effective mass $m_{eff} = 1.68 \times 10^{-18}$ kg, resonance frequency $f_0 = 28.47$ MHz, transduction responsivity $\Re = 105$ μV/nm, and $Q = 82$. Figure 2a depicts high amplitude driven resonance responses, whereas Figure 2b demonstrates the calibrated transmission and transduction responsivity (gain) of device 1 with increasing drive signal to the modulated laser. Such calibration measurements of transmission and transduction responsivity are detailed in Supporting Information S4 and S6. As can be seen in Figure 2a, the resonance frequency decreases with increasing drive amplitude as it goes into the nonlinear

https://doi.org/10.1021/acs.nanolett.2c02629
Nano Lett. XXXX, XXX, XXX−XXX

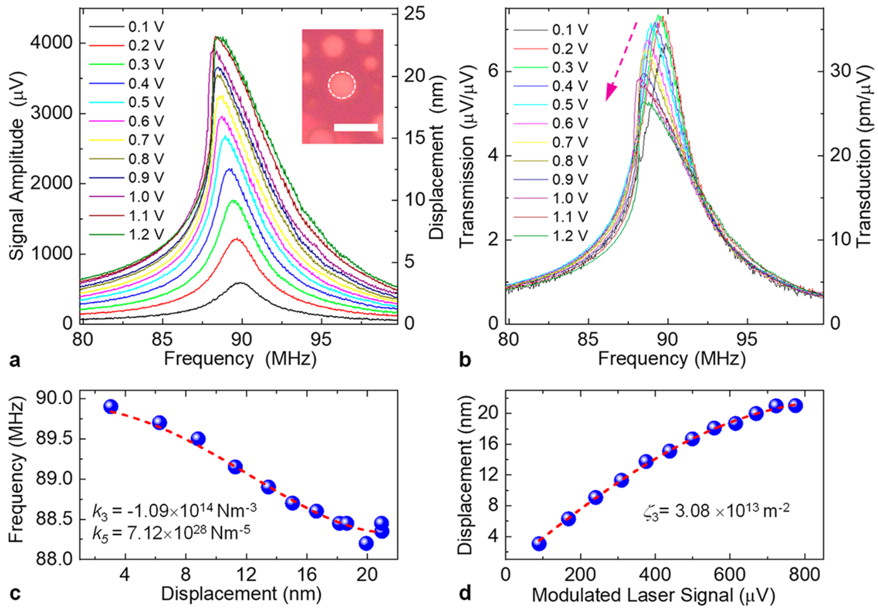

Figure 3. Determination of nonlinear damping and stiffness coefficients of a 2L MoS_2 resonator. (a) Signal amplitude and displacement with respect to frequency including device image identified by optical microscopy (inset, scale bar: 3 μm). (b) Transmission and transduction responsivity (gain) versus frequency. The dashed arrow indicates frequency pulling of the peak amplitude arising from nonlinear stiffness and damping. The peak transmission varies appreciably, indicating essentially nonlinear damping. (c) Frequency with respect to peak displacement (backbone curve). The red dashed line is a fit to eq 6. (d) Peak displacement versus modulated laser signal. The red dashed line is a fit to eq 7.

regime. This signifies that the 1L MoS_2 resonator (device 1) shows a softening effect with increasing RF drive.

Figure 2c shows the backbone curve, and we observe that the peak frequency of the 1L device drops as the displacement amplitude increases due to the softening effect. The red line is a curve fit to eq 6, and it well matches the experimental result. For the fitting analysis, we have kept the effective mass m_{eff} and eigenfrequency ω_0 as fixed parameters. Based on the curve fitting, a value is obtained for the Duffing coefficient, $k_3 = -2.21 \times 10^{13}$ N m^{-3}, and the quintic stiffness coefficient k_5 is nearly zero. The negative Duffing coefficient represents a softening effect. The softening nonlinearity can be attributed to geometrical nonsymmetries such as uneven tension or membrane bulging from the pressure difference between the cavity and chamber. Also, the focused laser on the suspended MoS_2 flake could introduce resonance motion-dependent laser heating, leading to a softening Duffing nonlinearity (Supporting Information section S10). The temperature increase by incident laser power generates thermal expansion and an attendant force on MoS_2 flake[31] as $F_{\text{ext}} = \beta(\Delta T_{405} + \Delta T_{633})$, where β converts the device temperature to thermal force. ΔT_{633} and ΔT_{405} are the temperature increases due to the 633 nm laser and the 405 nm modulated laser irradiation, respectively. The heating due to the 405 nm laser and the 633 nm probe laser are $\Delta T_{405}(t) = a_1 P_{405}\cos(\omega t)$ and $\Delta T_{633}(z) = a_2 P_{633}(z)$, respectively, where a_1 and a_2 convert the laser power to temperature change, and z is the vertical position of the membrane. The laser power spatial dependence for the standing wave is given by $P_{633}(z) = P_0\left(1 + R_{\text{Si}} - 2\sqrt{R_{\text{Si}}}\cos\left(\frac{4\pi z}{\lambda}\right)\right)$, where P_0, λ, and R_{Si} are the laser power, wavelength, and reflectivity of Si surface, respectively. Performing a Taylor expansion on P_{633} (z) using $\Delta z = z - z_0$ (z_0 is the equilibrium position for the membrane), one can obtain from eq 1

$$\ddot{x} + 2\zeta_1\omega_0\dot{x} + \frac{k_{\text{eff}} - \beta a_2 B}{m_{\text{eff}}}x - \frac{\beta a_2 C}{m_{\text{eff}}}x^2 + \frac{k_3 - \beta a_2 D}{m_{\text{eff}}}x^3 + \frac{k_5}{m_{\text{eff}}}x^5 = \frac{\beta(a_1 P_{405}\cos(\omega t) + a_2 A)}{m_{\text{eff}}} \tag{8}$$

where A, B, C, and D are the grouped coefficients whose values can be found in the Supporting Information (eq S20). For $k_{3,\text{eff}} = (k_3 - \beta a_2 D) < 0$, the third order x^3 term and also the x^2 term[32] both give softening nonlinearity in the 1L device.

With increasing input RF voltage, this device exhibits bifurcations and hysteresis, as supported by theory.[3] The nonlinearities in both damping and stiffness jointly affect the dynamic response of the system, for instance, the occurrence of hysteresis during frequency sweeps. For a system to exhibit multistability, the effect of nonlinear stiffness competes with both linear and nonlinear damping. In the limit of weak linear damping, if a given system can be adequately characterized using only cubic nonlinearities, then $k_3/\zeta_3 > 2m_{\text{eff}}\omega_0^2/\sqrt{3}$ can serve as a guide for the system's capability to exhibit bistability at sufficiently large amplitudes.[1,17] While this inequality should not be treated as an explicit criterion, since the system may be subject to factors including dynamic range, mode coupling, and other resonance, it is, however, able to provide a sensible estimate. In similar fashion, as the present work also studies quintic nonlinearities, another expression can be obtained using the method provided in ref 33. This bistability condition, which concerns quintic nonlinearities, is given by $k_5/\zeta_5 > 2m_{\text{eff}}\omega_0^2/\sqrt{5}$. For this 1L device, the nonlinear stiffness dominates the nonlinear effects, therefore, we observe hysteresis and clear bifurcations.

https://doi.org/10.1021/acs.nanolett.2c02629
Nano Lett. XXXX, XXX, XXX−XXX

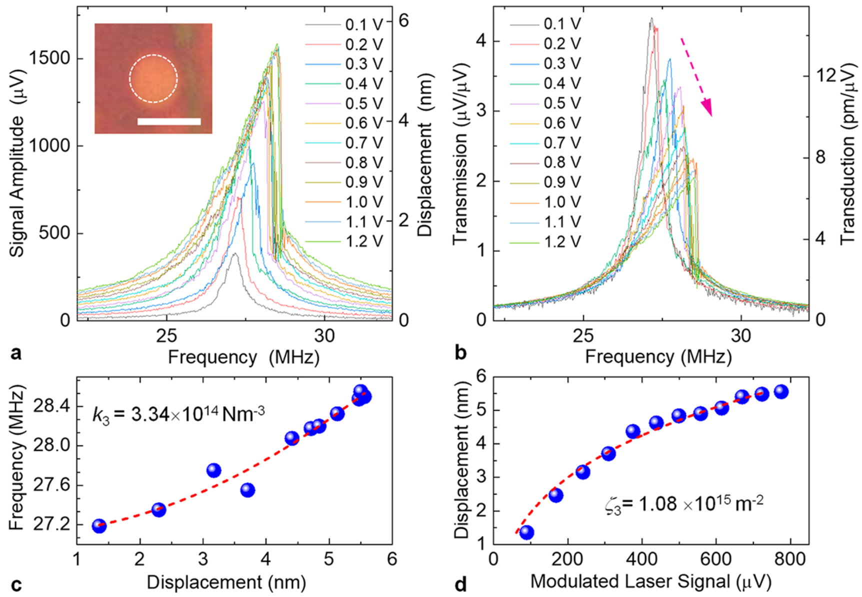

Figure 4. Determination of the nonlinear damping and stiffness coefficients of a 3L MoS_2 resonator. (a) Signal amplitude and displacement versus frequency with device image identified by optical microscopy (inset, scale bar: 2 μm). (b) Transmission and transduction responsivity (gain) versus frequency. The dashed arrow indicates frequency pulling of the peak amplitude arising from nonlinear stiffness and damping. The peak transmission varies appreciably, indicating essentially nonlinear damping. (c) Frequency with respect to peak displacement (backbone curve). The red dashed line is a fit to eq 6. (d) Peak displacement versus modulated laser signal. The red dashed line is a fit to eq 7.

Table 1. Measured and Extracted Device Parameters and Coefficients

	1Ldevice 1	2Ldevice 2	2Ldevice 3	2Ldevice 4	2Ldevice 5	3Ldevice 6
h (nm)	0.70	1.40	1.40	1.40	1.40	2.10
d (μm)	1.5	1.5	1.5	1.5	1.5	1.5
f_0 (MHz)	28.5	90.0	77.7	78.4	80.5	27.1
Q	82	38	42	42	51	70
$\mathfrak{R}$(μV/nm)	105	174	195	198	200	284
dynamic range (dB)	81	111	95	96	96	80
built-in tension, γ (N/m)	0.011	0.219	0.164	0.167	0.176	0.030
critical amplitude, x_c (nm)	5.7	17	3.5	3.8	4	3
m_{eff} (kg)	1.68×10^{-18}	3.37×10^{-18}	3.37×10^{-18}	3.37×10^{-18}	3.37×10^{-18}	5.05×10^{-18}
k_{eff}(N/m)	0.05	1.07	0.80	0.82	0.87	0.17
k_3(N m^{-3})	-2.24×10^{13}	-1.09×10^{14}	-3.22×10^{15}	-2.22×10^{15}	-9.09×10^{14}	3.34×10^{14}
$k_3x_c^3/k_{eff}x_c$	1.5%	3.0%	4.9%	3.9%	1.7%	1.8%
k_5(N m^{-5})	0	7.12×10^{28}	4.41×10^{31}	1.84×10^{31}	2.83×10^{30}	0
$k_5x_c^5/k_3x_c^3$	0	18.9%	16.8%	12.0%	5.0%	0
ζ_1	6.09×10^{-4}	1.32×10^{-2}	1.2×10^{-2}	1.19×10^{-2}	9.80×10^{-3}	7.14×10^{-3}
ζ_3 (m^{-2})	3.41×10^{12}	3.08×10^{13}	1.81×10^{15}	9.06×10^{14}	6.21×10^{14}	1.08×10^{15}

We have calibrated the amplitude of modulated laser signal (see Supporting Information, Figure S2) and then measured nonlinear responses of the device. Due to the low level of nonlinear damping in the 1L device, its peak displacement grows almost linearly with increasing modulated laser drive, as seen in Figure 2d. The red dashed line is a curve fit to eq 7, which is consistent with experimental data. For curve fitting of the data, we first keep the values of ζ_1, m_{eff}, and ω_0 as fixed parameters. Then we perform the fitting and obtain a value of the third order nonlinear damping coefficient of $\zeta_3 = 3.41 \times 10^{12}$ m^{-2}, whereas ζ_5 is found to be negligible and is assumed to be zero.

Figure 3 shows resonance response data measured from a 2L MoS_2 resonator (device 2) with large amplitude driven response, transmission, transduction responsivity, backbone curve, and curve fitting analysis. The device has $d = 1.5$ μm, $h = 1.4$ nm, $k_{eff} = 1.07$ N/m, $m_{eff} = 3.37 \times 10^{-18}$ kg, $f_0 = 89.9$ MHz, $\mathfrak{R} = 174$ μV/nm, and Q = 38. The softening effects observed in Figure 3a and 3b are similar to that shown in Figure 2. Figure 3c depicts the data and the curve fit for the stiffness coefficients from which it is determined that the value of Duffing coefficient is $k_3 = -1.09 \times 10^{14}$ N m^{-3} and the quintic coefficient is $k_5 = 7.12 \times 10^{28}$ N m^{-5}. From eq 8, it can be explained that the negative third-order stiffness and positive fifth-order stiffness (quintic) could lead to a mixed softening-hardening nonlinear behavior. For this 2L device (device 2), $k_3/\zeta_3 > 2m_{eff}\omega_0^2/\sqrt{3}$ and $k_5/\zeta_5 > 2m_{eff}\omega_0^2/\sqrt{5}$, so we observe hysteresis and evident bifurcations that are qualitatively the same as for the 1L device (device 1). Increasing the modulated laser signal results in a decrease in peak displacement

https://doi.org/10.1021/acs.nanolett.2c02629
Nano Lett. XXXX, XXX, XXX−XXX

amplitude when compared with the linear response, as shown in Figure 3d. In the 2L device (device 2), the nonlinear damping effect is more dominant than in the 1L device (device 1). We perform a curve fit analysis to obtain a value of ζ_3 = 3.08×10^{13} m^{-2} (one order higher in magnitude than for the 1L device), and again ζ_5 is found to be effectively zero.

We have also measured three other 2L devices (devices 3–5) where these are found to have quintic coefficient values of k_5 of 4.41×10^{31}, 1.84×10^{31}, and 2.83×10^{30} N m^{-5}, respectively. The nonlinear damping coefficients of these devices are in the range of 10^{14}–10^{15} m^{-2}, which are 1–2 orders of magnitude larger than the values for the 2L device 2. The quintic force of the 2L device 2 is around 20% of its Duffing force at displacement greater than 20 nm, so quintic coefficients cannot be neglected for these devices.

Figure 4 demonstrates resonance response data measured from a 3L MoS_2 resonator (device 6), with d = 1.5 μm, h = 2.1 nm, k_{eff} = 0.17 N/m, m_{eff} = 5.05×10^{-18} kg, f_0 = 27.1 MHz, $\mathfrak{R}$ = 284 μV/nm, and Q = 70. The data in Figure 4a reveals a hardening effect caused by membrane tensioning. As a result, in device 6, we observe that the stiffening Duffing nonlinearity dominates any softening effects present in this device. From Figure 4c, we determine k_3 = 3.34×10^{14} N m^{-3} and $k_5 \approx 0$. In 3L device 6, $k_3/\zeta_3 > 2m_{eff}\omega_0^2/\sqrt{3}$, so we observe hysteresis and clear bifurcations, similar to the 1L and 2L devices. Like the 2L devices (devices 2–5), Figure 4d indicates the effects of nonlinear damping in the 3L device. The curve fit yields ζ_3 = 1.08×10^{15} m^{-2} and $\zeta_5 \approx 0$.

Table 1 summarizes all measured and extracted parameters for the 1L, 2L, and 3L devices. In all cases, ζ_5 is negligible. The fitting lines well match the experimental data in all devices. We have found that quintic stiffness nonlinearity k_5 is needed to match eq 6 for all the 2L devices but not the 1L or 3L devices. This is the first direct measurement and analysis to confirm quintic stiffness nonlinearity in 2D NEMS resonators.

The Duffing coefficient for a circular membrane can be written as $k_3 = \frac{6.24\pi h E_Y}{d^2}\frac{13 + 21\nu - 4\nu^2}{30(1+\nu)}$, where h, d, E_Y, and ν are thickness, diameter, Young's modulus, and Poisson's ratio for 2D MoS_2.[40] Accordingly, the Duffing coefficient is proportional to the thickness and thus the number of layers of the MoS_2 device. In our experiments, however, we have both hardening due to membrane tensioning and softening from laser heating effects or asymmetric device parameters, so we have not found a systematic layer dependency in k_3. The mechanisms for other nonlinear coefficients in 2D NEMS (e.g., the quintic coefficient k_5 and nonlinear damping coefficients ζ_3, ζ_5) have not been explored yet, and the correlation between these parameters and the number of layers remains for future studies. In comparison with 1D nanotube and 1L graphene resonators,[16] note that the Duffing coefficient of a nanotube is k_3 = 4.80×10^{12} N m^{-3} and for a graphene resonator, k_3 = 1.40×10^{16} N m^{-3}. The 1L MoS_2 device here has a larger Duffing coefficient than that of the nanotube resonator, which is also shown in a previous study.[27]

To compare the nonlinear damping coefficient with prior results in the literature, we introduce the convenient parameter η for nonlinear damping, where $\eta = 2\zeta_3\omega_0 m_{eff}$. The nanotube and 1L graphene resonators[16] have values of η=7.90×10^5 kg m^{-2} s^{-1} and 1.50×10^7 kg m^{-2} s^{-1}, respectively, whereas our 1L (device 1), 2L (device 2), and 3L (device 6) devices have values of η = 2.05×10^3 kg m^{-2} s^{-1}, 1.17×10^5 kg m^{-2} s^{-1}, and 2×10^6 kg m^{-2} s^{-1}, respectively. In comparison to 1L graphene devices, the 1L MoS_2 device has a lower level of nonlinear damping. This could be due to geometric effects since our device is a circular membrane while the graphene device is a 1L rectangular sheet. Geometric parameters, such as cross-sectional area, moment of inertia, and Q factor can influence the nonlinear damping coefficient.[17] Another reason for the lesser nonlinear damping could be that our experiments have been carried out at room temperature, while the experiments in ref 16 were conducted at 4 K, and the value of the nonlinear damping coefficient decreases with rising temperature.[34] The intrinsic dissipation of 1L MoS_2 under axial and flexural modes of deformation can be determined from Akhiezer damping using molecular dynamics simulations, and it is found to be nonlinear and results from coupling between out-of-plane motion and in-plane stretching.[39] Whatever its source, the lower levels of nonlinear damping should be beneficial in 1L devices, corresponding to reduced frequency noise while vibrating at large amplitudes.[38]

In conclusion, we have presented an experimental demonstration of nonlinear damping, along with Duffing and quintic nonlinearities, in atomically thin MoS_2 nanomechanical resonators, and extracted the nonlinear stiffness and damping coefficients from resonance measurements. While nonlinearity imposes limits on dynamic range, it can also be employed in constructive ways, e.g., for reducing phase noise in oscillators,[35] developing improved threshold sensors,[36] and engineering transient responses.[37] In all cases, these nonlinear effects must be acknowledged and understood to utilize these devices in various emerging applications.

■ ASSOCIATED CONTENT

Supporting Information

The Supporting Information is available free of charge at https://pubs.acs.org/doi/10.1021/acs.nanolett.2c02629.

Device fabrication, laser interferometry measurement, calculation of motion transduction responsivity, calibration of input RF voltage to modulated laser signal, derivation of equation for resonance backbone curve and nonlinear damping, determination of transmission characteristics, procedure of fitting the backbone curve, procedure of fitting the nonlinear damping curve, theoretical estimation of Duffing nonlinear coefficient for circular membrane, laser-induced Duffing nonlinearity, frequency scaling and stress levels of MoS_2 nanomechanical resonators, and comparison of nonlinear coefficients with results in previous works (PDF)

■ AUTHOR INFORMATION

Corresponding Author

Philip X.-L. Feng – *Department of Electrical and Computer Engineering, Herbert Wertheim College of Engineering, University of Florida, Gainesville, Florida 32611, United States;* orcid.org/0000-0002-1083-2391; Email: philip.feng@ufl.edu

Authors

Tahmid Kaisar – *Department of Electrical and Computer Engineering, Herbert Wertheim College of Engineering, University of Florida, Gainesville, Florida 32611, United States;* orcid.org/0000-0002-7066-1993

Jaesung Lee – *Department of Electrical and Computer Engineering, Herbert Wertheim College of Engineering,* *University of Florida, Gainesville, Florida 32611, United States*

Donghao Li – *Department of Mechanical and Civil Engineering, Florida Institute of Technology, Melbourne, Florida 32901, United States*

Steven W. Shaw – *Department of Mechanical and Civil Engineering, Florida Institute of Technology, Melbourne, Florida 32901, United States; Departments of Mechanical Engineering and Physics & Astronomy, Michigan State University, East Lansing, Michigan 48423, United States*

Complete contact information is available at:
https://pubs.acs.org/10.1021/acs.nanolett.2c02629

Author Contributions

†Equally contributing authors

Notes

The authors declare no competing financial interest.

ACKNOWLEDGMENTS

We are thankful for the support from the National Science Foundation (NSF) CAREER Award (No. ECCS-2015708), NSF ECCS EPMD Program (No. ECCS-2015670), NSF CISE CCF-FET Program (No. CCF-2103091), NSF CMMI DCSD Program (No. CMMI-1662619), and BSF Program (No. 2018041).

REFERENCES

(1) Ye, F.; Islam, A.; Zhang, T.; Feng, P. X.-L. Ultrawide frequency tuning of atomic layer van der Waals heterostructure electromechanical resonators. *Nano Lett.* **2021**, *21*, 5508–5515.

(2) Samanta, C.; Arora, N.; Naik, A. K. Tuning of geometric nonlinearity in ultrathin nanoelectromechanical systems. *Appl. Phys. Lett.* **2018**, *113*, 113101.

(3) Lifshitz, R.; Cross, M. C. In *Review of Nonlinear Dynamics and Complexity*; Schuster, H., Ed.; Wiley: New York, 2008; Chapter 1.

(4) Aldridge, J. S.; Cleland, A. N. Noise-enabled precision measurements of a Duffing nanomechanical resonator. *Phys. Rev. Lett.* **2005**, *94*, 156403.

(5) Erbe, A.; Krömmer, H.; Kraus, A.; Blick, R. H.; Corso, G.; Richter, K. Mechanical mixing in nonlinear nanomechanical resonators. *Appl. Phys. Lett.* **2000**, *77*, 3102–3104.

(6) DeMartini, B. E.; Rhoads, J. F.; Turner, K. L.; Shaw, S. W.; Moehlis, J. Linear and nonlinear tuning of parametrically excited MEMS oscillators. *J. Microelectromech. Syst.* **2007**, *16*, 310–318.

(7) Polunin, P. M.; Yang, Y.; Dykman, M. I.; Kenny, T. W.; Shaw, S. W. Characterization of MEMS resonator nonlinearities using the ringdown response. *J. Microelectromech. Syst.* **2016**, *25*, 297–303.

(8) Rhoads, J. F.; Shaw, S. W.; Turner, K. L. Nonlinear dynamics and its applications in micro- and nano-resonators. *J. Dyn. Sys. Meas. Control.* **2010**, *132*, 034001.

(9) Lee, J.; LaHaye, M. D.; Feng, P. X.-L. Design of strongly nonlinear graphene nanoelectromechanical systems in quantum regime. *Appl. Phys. Lett.* **2022**, *120*, 014001.

(10) Xu, B.; Zhang, P.; Zhu, J.; Liu, Z.; Eichler, A.; Zheng, X.-Q.; Lee, J.; Dash, A.; More, S.; Wu, S.; Wang, Y.; Jia, H.; Naik, A.; Bachtold, A.; Yang, R.; Feng, X.-L.; Wang, Z. Nanomechanical resonators: toward atomic scale. *ACS Nano* **2022**, *16*, 15545–15585.

(11) Huang, X. M. H.; Zorman, C. A.; Mehregany, M.; Roukes, M. L. Nanodevice motion at microwave frequencies. *Nature* **2003**, *421*, 496.

(12) Feng, X. L.; White, C. J.; Hajimiri, A.; Roukes, M. L. A self-sustaining ultrahigh-frequency nanoelectromechanical oscillators. *Nat. Nanotechnol.* **2008**, *3*, 342–346.

(13) Nguyen, C. T.-C. Frequency-selective MEMS for miniaturized low-power communication devices. *IEEE Trans. Microw. Theory Technol.* **1999**, *47*, 1486–1503.

(14) Agarwal, M.; Mehta, H.; Candler, R. N.; Chandorkar, S. A.; Kim, B.; Hopcroft, M. A.; Melamud, R.; Bahl, G.; Yama, G.; Kenny, T. W.; Murmann, B. Scaling of amplitude-frequency-dependence nonlinearities in electrostatically transduced micro-resonators. *J. Appl. Phys.* **2007**, *102*, 074903.

(15) Kaajakari, V.; Mattila, T.; Oja, A.; Kiihamäki, J.; Seppä, H. Square extensional mode single-crystal silicon micromechanical resonator for low-phase-noise oscillator applications. *IEEE Electron Device Lett.* **2004**, *25*, 173–175.

(16) Eichler, A.; Moser, J.; Chaste, J.; Zdrojek, M.; Wilson-Rae, I.; Bachtold, A. Nonlinear damping in mechanical resonators made from carbon nanotubes and graphene. *Nat. Nanotechnol.* **2011**, *6*, 339–342.

(17) Zaitsev, S.; Shtempluck, O.; Buks, E.; Gottlieb, O. Nonlinear damping in a micromechanical oscillator. *Nonlinear Dyn.* **2012**, *67*, 859–883.

(18) Dykman, M. I.; Krivoglaz, M. A. Spectral distribution of nonlinear oscillators with nonlinear friction due to a medium. *Phys. Status Solidi B* **1975**, *68*, 111–123.

(19) Lee, H. K.; Melamud, R.; Chandorkar, S.; Salvia, J.; Yoneoka, S.; Kenny, T. W. Stable operation of MEMS oscillators far above the critical vibration amplitude in the nonlinear regime. *J. Microelectromech. Syst.* **2011**, *20*, 1228–1230.

(20) Buks, E.; Roukes, M. L. Electrically tunable collective response in a coupled micromechanical array. *J. Microelectromech. Syst.* **2002**, *11*, 802–807.

(21) Sato, M.; Hubbard, B. E.; Sievers, A. J.; Ilic, B.; Czaplewski, D. A.; Craighead, H. G. Observation of locked intrinsic localized vibrational modes in a micromechanical oscillator array. *Phys. Rev. Lett.* **2003**, *90*, 044102.

(22) Lee, J.; Wang, Z.; He, K.; Shan, J.; Feng, P. X.-L. High frequency MoS_2 nanomechanical resonators. *ACS Nano* **2013**, *7*, 6086–6091.

(23) Wang, Z.; Jia, H.; Zheng, X. Q.; Yang, R.; Ye, G. J.; Chen, X. H.; Feng, P. X.-L. Resolving and tuning mechanical anisotropy in black phosphorus via nanomechanical multimode resonance spectromicroscopy. *Nano Lett.* **2016**, *16*, 5394–5400.

(24) Ye, F.; Lee, J.; Feng, P. X.-L. Electrothermally tunable graphene resonators operating at very high temperature up to 1200 K. *Nano Lett.* **2018**, *18*, 1678–1685.

(25) Samanta, C.; Yasasvi Gangavarapu, P. R.; Naik, A. K. Nonlinear mode coupling and internal resonances in MoS_2 nanoelectromechanical system. *Appl. Phys. Lett.* **2015**, *107*, 173110.

(26) Güttinger, J.; Noury, A.; Weber, P.; Eriksson, A. M.; Lagoin, C.; Moser, J.; Eichler, C.; Wallraff, A.; Isacsson, A.; Bachtold, A. Energy-dependent path of dissipation in nanomechanical resonators. *Nat. Nanotechnol.* **2017**, *12*, 631–636.

(27) Manzeli, S.; Dumcenco, D.; Migliato Marega, G.; Kis, A. Self-sensing, tunable monolayer MoS_2 nanoelectromechanical resonators. *Nat. Commun.* **2019**, *10*, 4831.

(28) Davidovikj, D.; Alijani, F.; Cartamil-Bueno, S. J.; van der Zant, H. S. J.; Amabili, M.; Steeneken, P. G. Nonlinear dynamic characterization of two-dimensional materials. *Nat. Commun.* **2017**, *8*, 1253.

(29) Lee, J.; Wang, Z.; He, K.; Yang, R.; Shan, J.; Feng, P. X.-L. Electrically tunable single- and few-layer MoS_2 nanoelectromechanical systems with broad dynamic range. *Sci. Adv.* **2018**, *4*, eaao6653.

(30) Guckenheimer, J.; Holmes, P.Nonlinear oscillations, dynamical systems, and bifurcations of vector fields. In *Applied Mathematical Sciences*; Springer: New York, 1983, *42*.

(31) Ilic, B.; Krylov, S.; Craighead, H. G. Theoretical and experimental investigation of optically driven nanoelectromechanical oscillators. *J. Appl. Phys.* **2010**, *107*, 034311.

(32) Cho, H.; Jeong, B.; Yu, M.-F.; Vakakis, A. F.; McFarland, D. M.; Bergman, L. A. Nonlinear hardening and softening resonances in micromechanical cantilever-nanotube systems originated from nanoscale geometric nonlinearities. *Int. J. Solids Struct.* **2012**, *49*, 2059–2065.

(33) Li, D.; Shaw, S. W. The effects of nonlinear damping on degenerate parametric amplification. *Nonlinear Dyn.* **2020**, *102*, 2433−2452.
(34) Kumar, S.; Rebari, S.; Pal, S. P.; Yadav, S. S.; Kumar, A.; Aggarwal, A.; Indrajeet, S.; Venkatesan, A. Temperature-dependent nonlinear damping in palladium nanomechanical resonators. *Nano Lett.* **2021**, *21*, 2975−2981.
(35) Uranga, A.; Sobreviela, G.; Riverola, M.; Torres, F.; Barniol, N. Phase-noise reduction in a CMOS-MEMS oscillator under nonlinear MEMS operation. *IEEE Trans. Circuits Syst.-I: Regul. Pap.* **2017**, *64*, 3047−3055.
(36) Baguet, S.; Nguyen, V.-N.; Grenat, C.; Lamarque, C.-H.; Dufour, R. Nonlinear dynamics of micromechanical resonator arrays for mass sensing. *Nonlinear Dyn.* **2019**, *95*, 1203−1220.
(37) Miller, J. M. L.; Gomez-Franco, A.; Shin, D. D.; Kwon, H.-K.; Kenny, T. W. Amplitude stabilization of micromechanical oscillators using engineered nonlinearity. *Phys. Rev. Res.* **2021**, *3*, 033268.
(38) Ramshaw, J. D.; Lindenberg, K. Augmented Langevin description of multiplicative noise and nonlinear dissipation in Hamiltonian systems. *J. Stat. Phys.* **1986**, *45*, 295−307.
(39) De, S.; Kunal, K.; Aluru, N. R. Nonlinear intrinsic dissipation in single layer MoS_2 resonators. *RSC Adv.* **2017**, *7*, 6403−6410.
(40) Wang, Z.; Feng, P. X.-L. Dynamic range of atomically thin vibrating nanomechanical resonators. *Appl. Phys. Lett.* **2014**, *104*, 103109.

■ NOTE ADDED AFTER ASAP PUBLICATION

Due to a production error, this paper was published ASAP on December 8, 2022, with an error in Equation 5. The corrected version was reposted on December 9, 2022.

https://doi.org/10.1021/acs.nanolett.2c02629
Nano Lett. XXXX, XXX, XXX−XXX